journal

J. Am. Ceram. Soc., 77 [5] 1289–95 (1994)

Effect of Dopants on Zirconia Stabilization—An X-ray Absorption Study: III, Charge-Compensating Dopants

Ping Li* and I-Wei Chen*

Department of Materials Science and Engineering, University of Michigan, Ann Arbor, Michigan 48109-2136

James E. Penner-Hahn

Department of Chemistry, University of Michigan, Ann Arbor, Michigan 48109-1055

X-ray absorption spectra at the Zr-, Y-, and Nb-*K* edges of ZrO_2–$YNbO_4$ solid solutions have been measured at 10 K to determine the local atomic structures. Both Y and Nb cations substitute for Zr in the cation network but maintain rather different local oxygen coordination from Zr. In tetragonal zirconia solid solutions, Y adopts a YO_8 structure with a bond length of 2.32 Å. This is the same as the structure found in ZrO_2–Y_2O_3 solid solutions, confirming our previous conclusion that Y is not associated with oxygen vacancies. Nb has an NbO_4 structure with a bond length of 1.90 Å. This is shorter than the Zr–O_I distance of 2.10 Å. The strong Nb–O coordination increases the bonding disparity between Zr–O layers, thus increasing tetragonality. This is similar to the trend previously established for ZrO_2–GeO_2 solid solutions. Severe distortion of neighboring cations around the undersized Nb, similar to that previously found for undersized Fe^{3+} and Ga^{3+}, is also observed. At higher temperatures, local Y–Nb cation ordering occurs at a concentration below the solubility limit, similar to the Zr–Ge ordering reported previously. This cation ordering mechanism allows the charge-compensating Y–Nb pair to stabilize the tetragonal structure but increase tetragonality.

I. Introduction

FLUORITE-STRUCTURED oxides typically have considerable solubility for divalent, trivalent, and tetravalent cations, but their solubility for pentavalent cations is usually low. In CeO_2, the solubility on Nb_2O_5 is below 0.8 mol%.[1] For ZrO_2, very low solubility for Nb^{5+} and Ta^{5+} is also reported.[2,3] A much larger solubility, however, can be obtained if Nb^{5+} or Ta^{5+} is codoped with a divalent or trivalent cation, as demonstrated in the ZrO_2–MgO–Ta_2O_5[4] and ZrO_2–Y_2O_3–Ta_2O_5 systems.[5,6] Ionic conductivity measurements confirmed that, in the latter system, one oxygen vacancy was removed for every two Ta^{5+} added. Thus, the low solubility for Nb^{5+} and Ta^{5+} is obviously due to the difficulty in maintaining charge compensation by mechanisms other than oxygen vacancies in fluorite-structured oxides.

Addition of pentavalent cations to partially or fully stabilized zirconia, e.g., the ZrO_2–Y_2O_3 solid solutions, reduces the stability of the higher-temperature polymorphs (cubic and tetragonal) against distortion.[7,8] Since oxygen vacancies are effective in stabilizing both the cubic and tetragonal structures,[9] the destabilizing effect of Nb/Ta doping can be attributed to the decreased concentration of oxygen vacancies. The above reasoning, however, cannot be applied to the ZrO_2–$YNbO_4$/$YTaO_4$ system since oxygen vacancies are neither created nor annihilated. Nevertheless, the tetragonal phase of ZrO_2 is stabilized by the addition of $YNbO_4$/$YTaO_4$.[6,7] Interestingly, the tetragonality of the $YNbO_4$/$YTaO_4$-stabilized zirconia actually increases with additive concentration,[6,7,10] which is contrary to the observation for all of the divalent and trivalent cation-stabilized zirconia but reminiscent of the ZrO_2–GeO_2 solid solutions that we described in the preceding paper.[11] A clear explanation of these disparate phase-stabilizing, structure-distorting effects is not available in the current literature.

The purpose of this study is to use X-ray absorption spectroscopy to investigate the local atomic environments of Zr, Y, and Nb in zirconia solid solutions in order to obtain a better understanding of the above issues. Nb was chosen over Ta because its atomic number is similar to that of Zr and Y, which is important in maintaining nearly the same X-ray scattering environment regardless of alloy composition. Since Nb and Ta have essentially identical size and chemistry, the findings of this study should also be applicable to Ta-containing zirconia. The knowledge gained from this work will be combined with data from our previous studies of other solute cations[9,11] to provide a coherent picture of the role of stabilizing/destabilizing dopants in zirconia polymorphs. Additional background on the stability of zirconia and a complete list of references to previous EXAFS work on zirconia have been provided elsewhere.[9,11,12]

II. Experimental Procedure

(1) Materials

Ultrafine powders of zirconia with 10 and 20 mol% $YO_{1.5}$–$NbO_{2.5}$ ($YNbO_4$) were synthesized by a coprecipitation method using zirconium oxychloride, yttrium nitrate, and niobium ethoxide as starting materials, followed by drying at 250°C and calcination at various temperatures. The samples calcined at 850°C are designated as 10YNb08 and 20YNb08, with the first two digits indicating the mole percent of Y–Nb. A 10 mol% $YNbO_4$ sample calcined at 1400°C is designated as 10YNb14.

Phase identification and lattice parameter determination were made by X-ray diffraction (XRD). The results are summarized in Table I. With 10 and 20 mol% $YNbO_4$ addition and calcination at 850°C, a typical tetragonal zirconia XRD pattern could be identified in spite of peak broadening. With 10 mol% $YNbO_4$ and calcination at 1400°C, a single monoclinic zirconia pattern was observed. This phase is believed to be the product of tetragonal zirconia that transformed during cooling. When the concentration of $YNbO_4$ was increased to 20 mol% at 1400°C calcination temperature, both tetragonal and monoclinic zirconia were observed, along with a small amount of a monoclinic $YNbO_4$ phase. We believe that in this case the solubility limit of $YNbO_4$ in tetragonal zirconia was slightly exceeded, and during

W. White—contributing editor

Manuscript No. 194508. Received June 3, 1993; approved December 13, 1993.
Supported by the U.S. National Science Foundation under Grant No. DMR-91-19598. SSRL is operated by the Department of Energy, Office of Basic Energy Sciences, Division of Chemical Sciences, with additional support from the NIH, Biomedical Resource Technology Program, Division of Research Resources and the Department of Energy, Office of Health and Environmental Research.
*Member, American Ceramic Society.

Table I. Phase Identification of ZrO_2–$YNbO_4$ Samples

Sample	Phase	Lattice constants (Å)	c/a
10YNb08	*t*	$a = 5.105$	1.024
		$c = 5.227$	
20YNb08	*t*	$a = 5.114$	1.026
		$c = 5.249$	
10YNb14	*m*	$a = 5.167, b = 5.220$	
		$c = 5.337, \beta = 99.06°$	
20YNb14	$m + t + m$-$YNbO_4$		

cooling tetragonal zirconia partially transformed to the monoclinic phase. $YNbO_4$, which has a tetragonal fergusonite form with a scheelite-like structure at high temperature, apparently also transforms during cooling to a monoclinic form. The observation that the solubility of $YNbO_4$ in tetragonal zirconia at 1400°C is slightly below 20 mol% is in rough agreement with the literature. (At 1500°C, the solubility of $YTaO_4$ in tetragonal zirconia is reported to be about 22 mol%.[6]) The 20 mol% $YNbO_4$ solution that is maintained at 850°C is presumably a supersaturation because of the low diffusivity of cations at this temperature.

The unit cell of tetragonal zirconia (*a* and *c*) expands with the amount of $YNbO_4$, with the expansion in *c* being larger. Thus, the *c*/*a* ratio increases with increasing $YNbO_4$ concentration (see Table I). This result is in agreement with previous studies.[6,7,10] The unit cell (*a*, *b*, and *c*) of monoclinic zirconia (10YNb14) is also larger than that of pure *m*-ZrO_2, although the angular distortion (β) is similar. The above results confirm that solid solutions have been formed in 10YNb08, 20YNb08, and 10YNb14. These single-phase tetragonal and monoclinic zirconia powders were used in subsequent studies. In addition, pure ZrO_2, Y_2O_3, and Nb_2O_5 were investigated as model compounds.

(2) X-ray Absorption Measurements

X-ray absorption measurements at the Zr-, Y-, and Nb-*K* edges were performed using identical procedures as reported previously.[11,12] Spectra at 10 K were measured in transmission with the exception of Nb-*K* edge spectra for 10 mol% $YNbO_4$–ZrO_2 (10YNb08 and 10YNb14) which were measured in fluorescence mode using a multi-element Ge solid-state detector array. There is no phase transformation between ambient temperature and 10 K in these powdered specimens. The absorption spectrum of the corresponding pure oxide was recorded as an energy calibration standard at the same time as the sample spectrum. The calibration was defined by assigning the maximum inflection point of the Zr-*K* edge in ZrO_2 as 17998 eV, the Y-*K* edge in Y_2O_3 as 17038 eV, and the Nb-*K* edge in Nb_2O_5 as 18986 eV. Data analysis followed the same procedure as described in the preceding papers.[9,11–13] A quantitative analysis of the cation–oxygen shells was performed using theoretical amplitude and phase functions calculated using FEFF[14] with a distance parameter of 2.22 Å for a Zr–O pair, 2.28 Å for a Y–O pair, and 2.02 Å for a Nb–O pair to fit the corresponding cation–O shell. Energy values at $k = 0$, E_0, were initially assigned as 18015 eV for the Zr-*K* edge, 17055 eV for the Y-*K* edge, and 19005 eV for the Nb-*K* edge and then recalibrated so that the cation–O distance from the crystallographic data for pure oxides (2.16 Å for the Zr–O,[15] 2.28 Å for the Y–O,[16] and 2.02 Å for the Nb–O[17]) could be reproduced. The optimum E_0 value was 18034 eV for Zr EXAFS, 17076 eV for Y EXAFS, and 19023 eV for Nb EXAFS. These values for E_0 were then fixed for all subsequent analyses. Fourier-filter window values for the Zr–O, Y–O, and Nb–O shell are given in Table II. Theoretical amplitude and phase functions were calculated for Zr–Zr, Y–Zr, and Nb–Zr pairs using FEFF with a distance parameter of 3.62 Å. These were used to fit the corresponding Zr–, Y–, and Nb–cation shells. Since these three cations have almost identical scattering functions, the error induced by using a Zr shell to describe an alloy shell (Zr/Y/Nb) is negligible.

Table II. EXAFS Results of Cation–O Bonding in the ZrO_2–$YNbO_4$ System

$YNbO_4$–ZrO_2	Cation–O	*R* (Å)	CN*	σ^2 (Å^2)
10YNb08 (tetragonal)	Zr–O	2.10	4.0	0.0041
		2.36	4.0	0.0076
	Y–O	2.32	8.0	0.0112
	Nb–O	1.90	4.0	0.0036
20YNb08 (tetragonal)	Zr–O	2.10	4.0	0.0049
		2.33	4.0	0.0132
	Y–O	2.32	8.0	0.0090
	Nb–O	1.90	4.0	0.0048
10YNb14 (monoclinic)	Zr–O	2.16	7.0	0.0110
	Y–O	2.27	7.0	0.0072
	Nb–O	1.95	4.0	0.0056
		2.12	2.0	0.0029

*Fixed during fitting.

III. Results

(1) EXAFS Spectra of Cations

EXAFS spectra at the Zr-, Y-, and Nb-*K* edge for 10YNb08, 20YNb08, and 10YNb14 are shown in Figs. 1–3, respectively. For comparison, the EXAFS spectra for the reference oxides, ZrO_2, Y_2O_3, and Nb_2O_5, are also shown. Although the signal/noise ratio is excellent in all cases, only data up to $k = 14$–15 Å^{-1} are used for data analysis because of the presence of the Zr-*K* edge at 950 eV beyond the Y-*K* edge and the presence of the Nb-*K* edge at 988 eV beyond the Zr-*K* edge.

Zr^{4+} in each zirconia polymorph has a characteristic structure which is dopant-insensitive.[9,11,12] In Fig. 1 we see that the spectra at the Zr-*K* edge are indistinguishable for pure ZrO_2 and 10YNb14, which are both monoclinic. Likewise, the spectra for 10YNb08 and 20YNb08, which are both tetragonal, are mutually similar. The decrease in EXAFS amplitude for 20YNb08 relative to 10YNb08 is attributed to structural disorder due to random alloying.[9,11]

Turning to the Y edge, we can differentiate three types of EXAFS spectra in Fig. 2 which correspond to three different phases, C-type Y_2O_3, tetragonal 10YNb08 and 20YNb08, and monoclinic 10YNb14. Likewise, the Nb EXAFS as shown in Fig. 3 can be grouped by their phases, Nb_2O_5, tetragonal 10YNb08 and 20YNb08, and monoclinic 10YNb14. Thus, the local environments around dopants are phase-dependent.[9,11,13] The Y and Nb EXAFS amplitudes for 20YNb08 are also damped relative to those for 10YNb08 due to structural disorder.

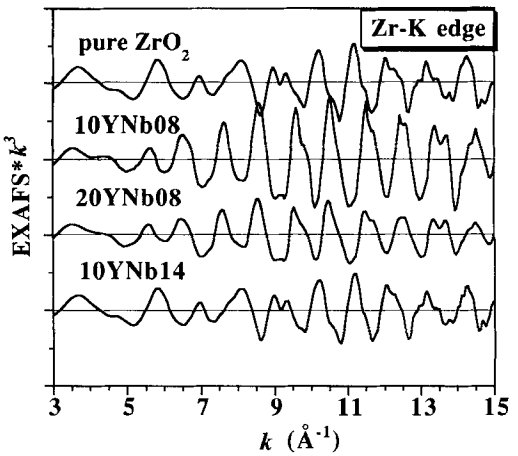

Fig. 1. EXAFS spectra at Zr-*K* edge for *m*-ZrO_2 and ZrO_2–$YNbO_4$ solid solutions.

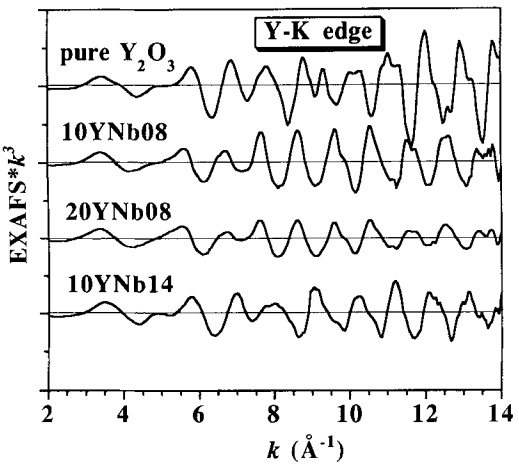

Fig. 2. EXAFS spectra at Y-*K* edge for Y_2O_3 and ZrO_2–$YNbO_4$ solid solutions.

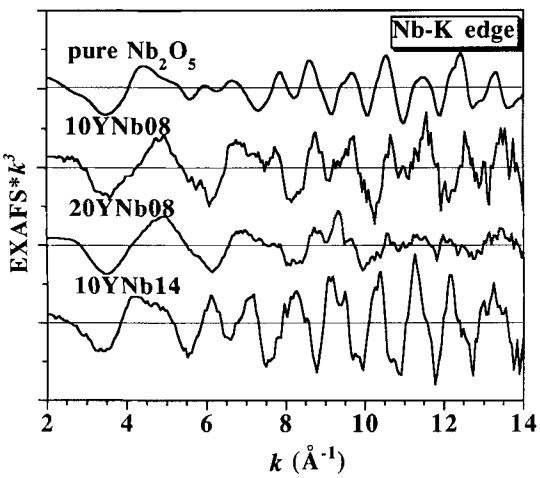

Fig. 3. EXAFS spectra at Nb-*K* edge for Nb_2O_5 and ZrO_2–$YNbO_4$ solid solutions.

(2) *Pseudoradial Distribution Functions around Cations*

(A) Tetragonal Zirconia: Fourier transforms (FTs) of the Zr, Y, and Nb EXAFS for tetragonal 10YNb08 and 20YNb08 are shown in Figs. 4 and 5. Since Y^{3+}, Zr^{4+}, and Nb^{5+} are isoelectronic and have almost identical scattering and phase functions, the Fourier transforms, as pseudoradial distribution functions of the absorber atoms,[18] can be directly used to compare the structures surrounding each ion. Specifically, the first peak in the FTs corresponds to the nearest neighbors (NN) around the probe cation (Zr–O, Y–O, or Nb–O), and the second peak corresponds to the next-nearest neighbors (NNN), i.e., Zr–cation, Y–cation, or Nb–cation. The higher-order peaks correspond to outer cation–cation shells.

Comparing these FTs, we find a noticeable two-subshell feature in the Zr–O peak in both 10YNb08 and 20YNb08, with the outer subshell much weaker in the latter. In contrast, there is only a single resolved cation–O peak for the Nb and Y EXAFS. Relative to the Zr–O inner shell, the Nb–O shell has a shorter distance and the Y–O shell has a longer distance. Since Zr, Y, and Nb have very similar cation–cation (NNN) distances, both Y and Nb substitute for Zr in the Zr–cation network in tetragonal zirconia solid solutions.

The much lower amplitude of the Nb–NNN peak than those of the Y and Zr–NNN peaks in both compositions indicates a significant distortion in the Nb-centered cation network. Similarly, but to a lesser extent, the Y–cation shell is more distorted (lower FT amplitude) than the Zr–cation shell. This was also

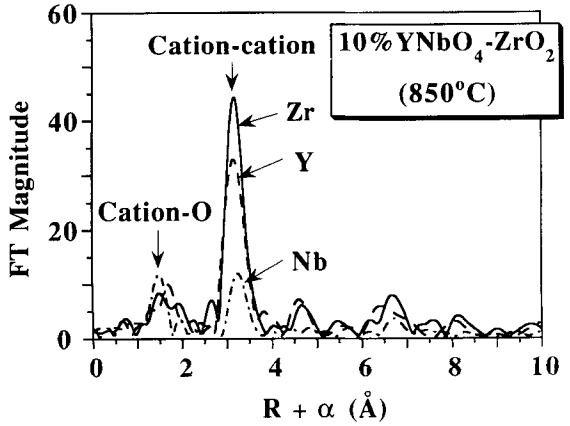

Fig. 4. Fourier transforms of Zr, Y, and Nb EXAFS for *t*-ZrO_2 stabilized by 10 mol% $YNbO_4$ (calcined at 850°C).

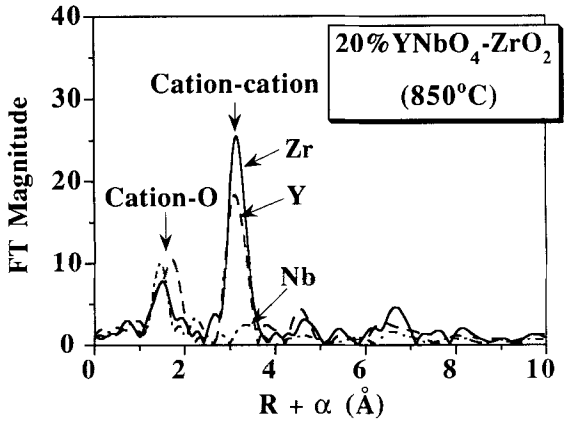

Fig. 5. Fourier transforms of Zr, Y, and Nb EXAFS for *t*-ZrO_2 stabilized by 20 mol% $YNbO_4$ (calcined at 850°C).

found in the tetragonal ZrO_2–Y_2O_3 at 10 K.[13] The amplitudes of all of the cation networks are significantly smaller for 20YNb08, a "normal" behavior[11] because of the increased distortion of the cation network at the higher $YNbO_4$ concentration.

Quantitative fitting results for the cation–O shells are given in Table II. Two sets of bond lengths, 2.10 and 2.33–2.36 Å, are found for the Zr–O shell in both 10YNb08 and 20YNb08. These values are characteristic of tetragonal zirconia.[9-11] The Debye–Waller factors (σ^2) suggest that the distortion of the Zr–O shell increases with increasing dopant concentration. The larger σ^2 for the outer Zr–O subshell reflects, in particular, a weaker bond strength.[9,11,12,19] In 20YNb08, σ^2 is so large that the size of the shoulder on the high-*R* side of the Zr–O peak is very weak (Fig. 5).

A bond length of 2.32 Å with 8-fold coordination is found for the Y–O shell in both of the tetragonal solid solutions. These results are also characteristic of Y in tetragonal zirconia.[9,13] The relatively high bond dispersion indicates a very distorted environment around the Y. A much shorter bond length (1.90 Å) and lower (4-fold) coordination are found for the Nb–O shell reflecting a much smaller ionic size of Nb. (For the coordination number, we first fit the EXAFS data without fixing the coordination. We then choose from among those results that give a satisfactory fit, a chemically reasonable coordination number. This number is fixed in subsequent fitting to obtain the other quantities listed in Table II. The result of 4-fold coordination for Nb–O implies that only four oxygens are close to Nb. Other oxygens may be too loosely bound to be visible in EXAFS. (This coordination number is also supported by the following discussion.) Note that the Y–O bond length (2.32 Å) in the

doped zirconia is larger than that (2.28 Å) in Y_2O_3, while the Nb–O bond distance (1.90 Å) is smaller than that (2.02 Å) in Nb_2O_5. These results are consistent with the change of coordination number (6 to 8 for Y and 6 to 4 for Nb; from pure oxide to zirconia solid solution). These M–O distances are also in agreement with those found in tetragonal fergusonite ($YNbO_4$), which has a coordination number 8 for Y and 4 for Nb.[20] Interestingly, the distortion of the Y–O shell decreases with increasing concentration of dopant ($YNbO_4$). In contrast, the distortion of the Nb–O shell behaves "normally"; i.e., it increases with increasing dopant concentration. Finally, a quantitative analysis of the second peak in Figs. 4 and 5 shows that the cation–cation distance is essentially the same for all three cations. This distance (3.62 Å) is characteristic of the Zr–Zr distance in tetragonal zirconia,[12] again confirming that these three cations form a solid solution.

(B) Monoclinic Zirconia: Fourier transforms of the Zr-, Y-, and Nb-*K* edge EXAFS for 10YNb14 are shown in Fig. 6. The cation–cation shells (the second peaks in Fig. 6) are now split into three subshells, with their distances approximately the same for all three cations. The peaks correspond well with the peaks in pure monoclinic ZrO_2 but not with those in Nb_2O_5 and Y_2O_3 (Fig. 7). This, together with the XRD results, suggests that both Y and Nb have dissolved into the Zr network and formed a monoclinic zirconia solid solution. Since the monoclinic phase results from a diffusionless transformation of the tetragonal phase during cooling, it also implies that the Zr, Y, and Nb form a solid solution in tetragonal structure at 1400°C, in agreement with our observation for 10YNb08. (The lower stability of 10YNb14 compared to 10YNb08 is most likely due to a larger particle size after high-temperature calcination, favoring monoclinic nucleation.[21]) Interestingly, a larger amplitude is found for the Y–cation shell relative to those for Zr and Nb. This indicates a less distorted Y-centered cation network in the monoclinic solid solution. Even more interesting is the fact that the amplitude of the Nb–cation shell is actually very strong in this monoclinic sample whereas it is very weak in both of the tetragonal samples (Figs. 4 and 5). These observations are "abnormal" for a random solid solution[11] and suggest that Y–Nb ordering has occurred at high temperature in the tetragonal phase, and, through phase transformation, this ordered structure is inherited in the monoclinic phase.

Quantitative analysis gives the results shown in Table II. The Zr–O shell data are consistent with our previous studies of characteristic structure in the monoclinic zirconia.[9,12] The Y–O shell is also 7-fold coordinated, with a bond length of 2.27 Å. In contrast, two peaks are found for the Nb–O shell, with bond distances at 1.95 and 2.12 Å and a total coordination number of 6. Note that while the mean bond lengths of both Zr–O and Y–O are shorter in monoclinic zirconia solid solution than in tetragonal zirconia, the opposite is true for the Nb–O bonds. This is consistent with the decrease in the average coordination number for Zr (8 to 7) and Y (8 to 7) and the increase in the average coordination number for Nb (4 to 6) from tetragonal to monoclinic zirconia.

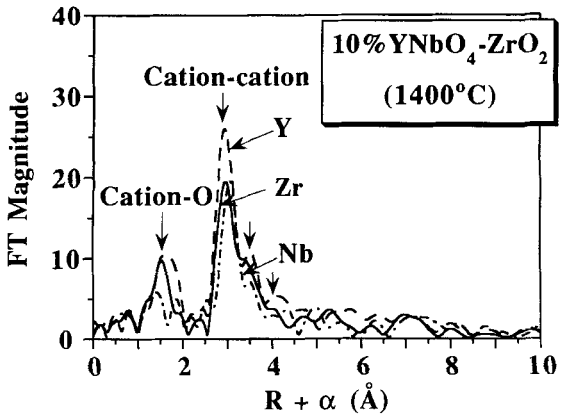

Fig. 6. Fourier transforms of Zr, Y, and Nb EXAFS for *m*-ZrO_2 containing 10 mol% $YNbO_4$ (*t*-to-*m* transformation during cooling after 1400°C calcination).

(3) XANES Spectra

X-ray absorption near-edge (XANES) spectra at the Zr-, Y-, and Nb-*K* edges for 10YNb08, 20YNb08, and 10YNb14 are shown in Figs. 8–10, respectively. The spectra at each edge are similar for 10YNb08 and 20YNb08, which are both tetragonal, but significantly different for 10YNb14, which is monoclinic. Thus, the XANES spectra are also phase dependent. The main peak in the *K*-edge spectrum is due to transitions into *p*-symmetry final states.[22] This occurs when a positively charged (core) hole remains sufficiently unshielded so that it binds the *p* states and produces exciton levels. This includes both atomic-like transitions (e.g., $1s \rightarrow 5p$) and "continuum resonances" where the X-ray excited photoelectron is weakly bound by the repulsive potential of the surrounding scatterers.[23] These XANES features are sensitive primarily to the symmetry and bond length around cations. The disorder in the Nb site (cf. second peak in Figs. 4 and 5) is therefore expected to give a broad range of continuum resonance energies for the samples calcined at 850°C. The ordering of Y and Nb at 1400°C should sharpen these energy spectra for all three elements, especially for Nb. This trend is clearly manifested in Figs. 8–10. The systematic differences in shape between Y and Zr for the 850°C samples may reflect differences in the relative importance of $1s \rightarrow 5p$ and $1s \rightarrow$ continuum resonance, with the latter (higher energy) transition being less important for the more disordered Y sites.

A small shoulder about 6 eV below the principal peak is marked by an arrow in each figure. It is visible for the Zr edge, more apparent for the Nb edge, but barely resolved for the Y edge in the tetragonal samples. This pre-edge feature is absent in the monoclinic sample. In general, XANES features within ca. 10 eV below the edge threshold are due to electronic transitions to unoccupied high-energy states near the Fermi level.[22] These transitions are particularly sensitive to the local geometry (first anion neighbors in ionic compounds) of the probe atom. Thus, the difference in the shoulders for Zr, Y, and Nb suggests that there are different cation–O geometries for the different cations. Since we have attributed the principle peak of the *K* edge to a $1s \rightarrow 5p$ dipole-allowed transition, the shoulder in the rising edge may be attributed to a mixing of unoccupied *d* final states with *p*-character final states. Such *d–p* mixing is forbidden for a centrosymmetric (e.g., octahedral) environment but is allowed in a noncentrosymmetric (e.g., tetrahedral) environment. Thus, a roughly tetrahedral environment in Nb–O in tetragonal solid solutions (Table II) gives a relatively strong shoulder on the Nb edge in 10YNb08 and 20YNb08. Further support for this interpretation comes from our recent study of perovskite niobate structures,[24] which have an octahedral NbO_6 environment and hence no XANES shoulder. The same reasoning can also apply for Zr for which tetrahedral-like structures are present only in tetragonal zirconia due to a splitting of ZrO_8 bonding.[12] Correspondingly, a weak shoulder on the Zr edge is characteristic of all the XANES spectra of tetragonal solid solutions (Fig. 8). Other than the above two cases, the remaining cation–O geometries (the 7-fold Zr–O and Y–O coordination in the monoclinic phase, the 6-fold coordination for Nb–O in the monoclinic phase, as well as the YO_8 cubiclike structure in the tetragonal phase) apparently have small *d–p* orbital mixing and thus do not have detectable shoulders on the rising edge.

IV. Discussion

(1) Local Atomic Structures in ZrO_2–$YNbO_4$

It has been questioned previously whether Nb (and Ta) occupies substitutional[5] or interstitial sites in Y-stabilized zirconia solid solutions.[6] The present results unequivocally support the

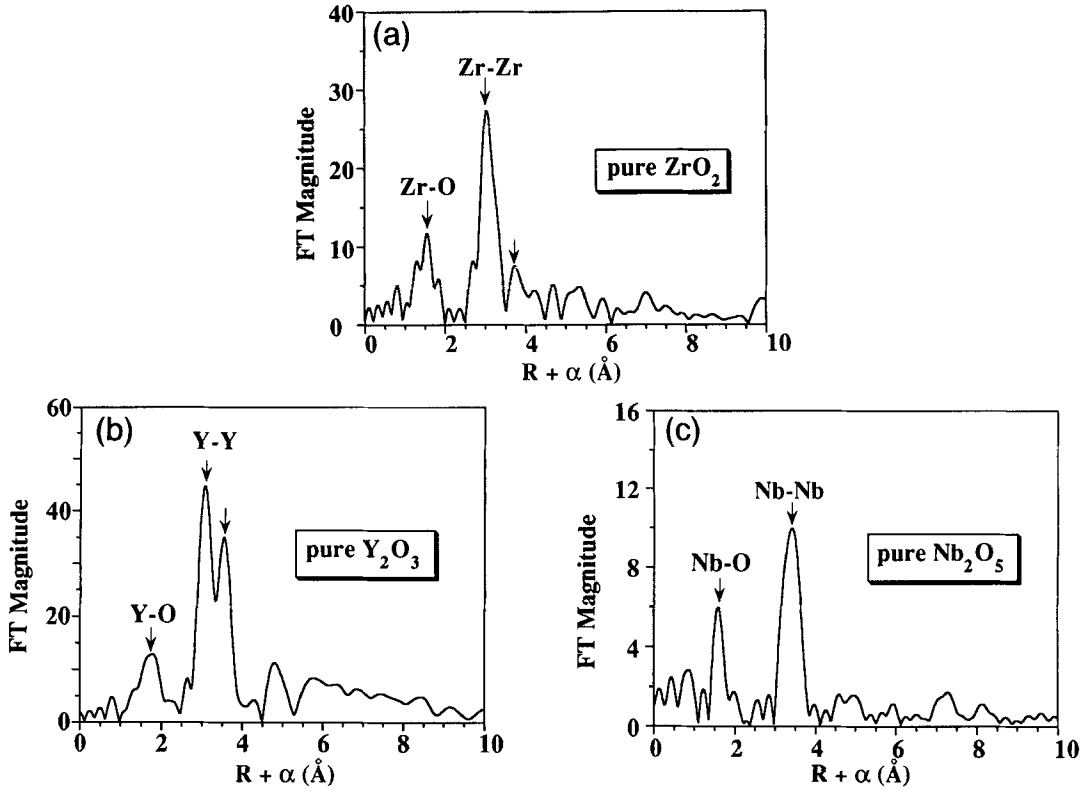

Fig. 7. Fourier transforms of (a) Zr EXAFS for *m*-ZrO_2, (b) Y EXAFS for Y_2O_3, and (c) Nb EXAFS for Nb_2O_5.

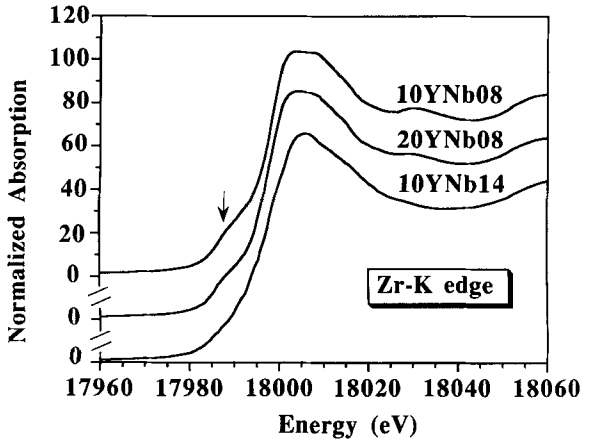

Fig. 8. XANES spectra at Zr-*K* edge for *m*- and *t*-ZrO_2 containing $YNbO_4$ (shifted vertically for clarity).

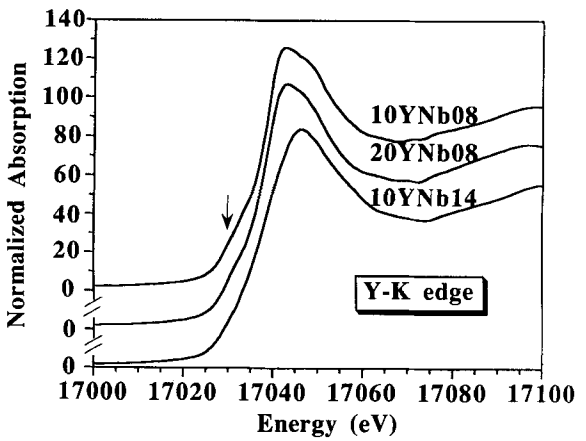

Fig. 9. XANES spectra at Y-*K* edge for *m*- and *t*-ZrO_2 containing $YNbO_4$ (shifted vertically for clarity).

substitutional model. This solid solution is mostly disordered at low temperature, causing more distortion with increasing Y–Nb dopant concentration (e.g., Figs. 4 and 5). At higher temperatures, Y and Nb become ordered, causing a substantial decrease in the cation–cation distortion, particularly for Nb. A similar ordering process with a similar change in the amplitude of EXAFS was observed for the ZrO_2–GeO_2 system described in the preceding paper.[11] In both cases ordering occurs at concentrations well below the solubility limit.

Theoretically, ordering in a binary alloy must involve both host (Zr) and solute (Ge) cations, whereas ordering in a ternary alloy could conceivably involve only solute cations, not Zr. This latter option is apparently exercised in the ZrO_2–$YNbO_4$ system. Indeed, at higher Y–Nb concentrations (e.g., 20% $YNbO_4$), an ordered phase of monoclinic $YNbO_4$ was observed after 1400°C calcination. It is also conceivable that ordering preferentially starts around one cation only. For example, Nb cations may migrate to take up certain preferred sites around Y, whereas Y remains randomly distributed. Some evidence in support of this scenario is seen in the "abnormal" Y–O distortion which decreases with increasing dopant concentration for 10YNb08 and 20YNb08. The Nb–O distortion is "normal" for these samples. More fully developed ordering eventually obtains at higher temperatures when Y cations become mobile. However, even in this case, it is still possible that ordering around Y is more complete than that around Nb. This could account for the larger amplitude of the Y–cation shell for 10YNb14. Similar kinetic consideration can also explain why ordering does not take place in 10YNb08 but in 10YNb14, since diffusivity may be too low at low temperature despite a possibly larger driving force.

Dopant–oxygen bond lengths are very different from the Zr–O distance, even in solid solutions. This is a general result for all of the dopants that we have investigated.[9,11] The bond

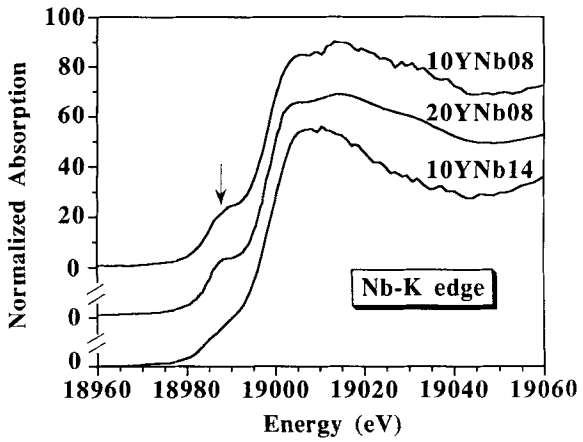

Fig. 10. XANES spectra at Nb-*K* edge for *m*- and *t*-ZrO_2 containing $YNbO_4$ (shifted vertically for clarity).

length of 2.32 Å for Y–O is a direct measurement of bond length for 8-fold-coordinated Y. (There are no oxygen vacancies in ZrO_2–$YNbO_4$.) Smaller than suggested by Shannon's radii,[25] it is, nevertheless, consistent with the diffraction data for tetragonal $YNbO_4$[20] and is identical to the Y–O bond length in tetragonal and cubic zirconia,[9,13] all of which have YO_8 polyhedra. In the monoclinic zirconia, the Y–O distance decreases to 2.27 Å, also consistent with MO_7 polyhedra in monoclinic zirconia.

The Nb–O bonding favors an NbO_4 polyhedron in tetragonal zirconia. The Nb–O distance (1.90 Å) in the tetragonal zirconia is actually shorter than the Zr–O_I bond length (2.10 Å) in the same structure, causing increased tetragonality as discussed in the next subsection. In monoclinic zirconia, the prevalence of MO_7 polyhedra for Zr and Y seems to force the Nb to adopt a longer average bond length and a higher coordination number. This latter structure is more reminiscent of the parent, and probably more natural, Nb_2O_5 structure. Lastly, in the absence of ordering, the undersized Nb causes severe distortion of the surrounding cation network. This feature is characteristic of other undersized dopants of zirconia solid solutions.[9]

(2) Role of Nb^{5+} in Stabilizing Zirconia

Stabilization of the fluorite-type zirconia lattice can be achieved either by oxygen vacancies or by cation network stabilizers. Trivalent dopants stabilize zirconia by the first mechanism,[9,13] whereas tetravalent dopants stabilize zirconia by the second mechanism.[11] Nb doping and Y–Nb codoping provide an interesting example that involves both mechanisms.

At low dopant concentrations, Nb and Ta are destabilizers for Y-stabilized tetragonal and cubic zirconia[6–8] because they annihilate the oxygen vacancies introduced by Y^{3+}. Atomistically, this occurs by forming NbO_4, TaO_4, YO_8, and ZrO_8, in place of ZrO_7. The decreased concentration of ZrO_7 is directly responsible for the decreased stability of the tetragonal and cubic phases. The removal of oxygen vacancies also has the effect of increasing the tetragonality[7,8] since the anisotropy of the layer structure of tetragonal zirconia, as supported by the Zr–O_I and Zr–O_{II} bifurcation, becomes stronger without the disruption of Zr-associated oxygen vacancies.[11]

Codoping of Y and Nb to high concentrations has an effect similar to that of Ge doping. In both cases, they stabilize tetragonal zirconia and increase tetragonality without introducing oxygen vacancies. The cations in both cases tend to order into a common, scheelite-like structure. In the ordered structure, the smaller cations, Nb and Ge, respectively, adopt a 4-fold coordination leaving 8-fold coordination to the larger cations, and the pattern for cation partition is layerlike. In particular, since the Ge–O and Nb–O distances are shorter than the Zr–O_I distance, the bonding anisotropy of the layerlike structure is accentuated, resulting in higher tetragonality. A probable cause for the ordering[11] is the reduction in strain energy of the highly unstable, internally strained tetragonal lattice, whose instability is rooted in the unfavorable ZrO_8 configuration for the relatively small Zr cations. With the aid of an even smaller cation species which adopts 4-fold coordination, a more favorable packing in the form of an ordered layerlike structure becomes possible and the oxygen overcrowding around Zr is alleviated. The present observation supports this model.

Ordering involving the smallest (Nb) and largest (Y) cations is apparently sufficient to partially stabilize tetragonal zirconia. The stabilizing effect of $YNbO_4$, however, is less than that of GeO_2 for two reasons. First, since ordering in the ZrO_2–$YNbO_4$ system probably extends only to Y and Nb and not to Zr, the reduction of strain energy is obviously smaller for ZrO_2–$YNbO_4$. Second, tetragonal $YNbO_4$ is itself an unstable structure that undergoes a tetragonal-to-monoclinic distortion during cooling.[26,27] This is unlike ZrO_2–GeO_2 alloys, Zr_3GeO_8 and $ZrGeO_4$, which are stable in the tetragonal form at all temperatures. This expectation of decreased stabilization is in broad agreement with the experimental transformation temperatures.[6,7,28] Lastly, a comparison of the tetragonality of $YNbO_4$ (0.0605),[27] Zr_3GeO_8 (0.0442),[29] $ZrGeO_4$ (0.0841),[29] and *t*-ZrO_2 (0.0202)[30] is instructive. At a comparable Nb/Ge atomic fraction, the tetragonality of $YNbO_4$ is less than that of $ZrGeO_4$. Likewise, the effect of $YNbO_4$ doping on the tetragonality of *t*-ZrO_2 is less than that of GeO_2 doping. (The increase in tetragonality is 0.0002 per mol% Nb doping versus 0.0005 per mol% Ge doping.) Using our model, these differences are understandable given the different bond distances (1.90 Å for Nb–O versus 1.81 Å for Ge–O) and hence bond strengths (stronger for Ge–O) for the two dopants.

V. Conclusions

(1) ZrO_2 and $YNbO_4$ form a substitutional solid solution in both tetragonal and monoclinic form. All three cations (Zr, Y, and Nb) have a similar cation–cation distance but very different cation–oxygen coordination. This is consistent with the behavior of other substitutional solid solutions.[9,11]

(2) Nb in tetragonal zirconia is tetrahedrally coordinated with a shorter Nb–O bond length than that of Zr–O_I. In random distribution, this undersized cation causes severe distortion in its surrounding cation environment as evidenced by a very weak EXAFS amplitude associated with Nb–cation scattering. This is also consistent with the behavior of other undersized dopants in zirconia solid solutions.[9]

(3) Y in tetragonal zirconia has 8-fold oxygen coordination with a distance of 2.32 Å. This is in agreement with our previous study of this system in the tetragonal and cubic form in the absence of Nb. The direct verification of the Y–O distance in 8-fold coordination lends support to our structural picture that oxygen vacancies in ZrO_2–Y_2O_3 are not associated with Y.[9,13]

(4) Y–Nb ordering in tetragonal zirconia into a scheelite-like arrangement probably takes place at high temperatures (1400°C in this study) and well within the solubility limit. The ordering reduces the large strain energy inherent in the *t*-ZrO_2 structure. The ordered structure is layerlike and the 4-fold-coordinated Nb–O bonding is stronger than that of Zr–O_I, resulting in an increase in the anisotropy of the parent *t*-ZrO_2 layer structure and its tetragonality. This picture is consistent with that used to explain the stability and tetragonality of ZrO_2–GeO_2 solid solution, where Ge also favors tetrahedral coordination.

References

[1]I. K. Naik and T. Y. Tien, "Electrical Conduction in Nb_2O_5-doped Cerium Dioxide," *J. Electrochem. Soc.*, **126** [4] 562–66 (1979).

[2]R. S. Roth and L. W. Coughanour; p. 144 in *Phase Diagram for Ceramists*, Vol. 1. Edited by E. M. Levin, C. R. Robbins, and H. F. McMurdie. American Ceramic Society, Columbus, OH, 1964.

[3]B. W. King, J. Schulz, E. A. Durbin, and W. H. Duckworth; p. 144 in *Phase Diagram for Ceramists*, Vol. 1. Edited by E. M. Levin, C. R. Robbins, and H. F. McMurdie. American Ceramic Society, Columbus, OH, 1964.

[4]S. Prietzel, L. J. Gauckler, and G. Petzow, "Stabilizing of Cubic ZrO_2 in the System ZrO_2–MgO–Ta_2O_5 and Its Electrical Conductivity"; pp. 725–30 in *Science of Ceramics*, Vol. 9. Edited by H. Hausner. Deutsche Keramische Gesellschaft, Weiden, Germany, 1980.

[5]C. B. Choudhary and E. C. Subbarao, "Electrical Conduction in the Cubic Fluorite Phase in the System ZrO_2–$YO_{1.5}$-$TaO_{2.5}$"; pp. 665–68 in *Fast Ion Transport in Solids*. Edited by P. Vashishta, J. N. Mundy, and G. K. Shenoy. Elsevier/North-Holland, New York, 1979.

[6]D. J. Kim and T. Y. Tien, "Phase Stability and Physical Properties of Cubic and Tetragonal ZrO_2 in the System ZrO_2–Y_2O_3–Ta_2O_5," *J. Am. Ceram. Soc.*, **74,** 3061–65 (1991).

[7]D. J. Kim, "The Effect of Alloying on the Transformability of Y_2O_3 Stabilized Tetragonal ZrO_2"; Ph.D. Thesis. University of Michigan, Ann Arbor, MI, 1988.

[8]D. J. Kim, "Effect of Ta_2O_5, Nb_2O_5 and HfO_2 Alloying on the Transformability of Y_2O_3-Stabilized Tetragonal ZrO_2," *J. Am. Ceram. Soc.*, **73,** 115–20 (1990).

[9]P. Li, I-W. Chen, and J. E. Penner-Hahn, "The Effect of Dopants on Zirconia Stabilization—An X-ray Absorption Study: I, Trivalent Dopants," *J. Am. Ceram. Soc.*, **77** [1] 118–28 (1993).

[10]T. S. Sheu, "Phase Stability of Zirconia Solid Solutions"; Ph.D. Thesis. University of Michigan, Ann Arbor, MI, 1989.

[11]P. Li, I-W. Chen, and J. E. Penner-Hahn, "The Effect of Dopants on Zirconia Stabilization—An X-ray Absorption Study: II, Tetravalent Dopants," *J. Am. Ceram. Soc.*, **77** [5] 1281–88 (1994).

[12]P. Li, I-W. Chen, and J. E. Penner-Hahn, "X-ray Absorption Studies of Zirconia Polymorphs. I. Characteristic Local Structure," *Phys. Rev. B*, **48** [14] 10063–73 (1993).

[13]P. Li, I-W. Chen, and J. E. Penner-Hahn, "X-ray Absorption Studies of Zirconia Polymorphs. II. Effect of Y_2O_3 Dopant on Zirconia Structure," *Phys. Rev. B*, **48** [14] 10074–81 (1993).

[14]J. J. Rehr, J. Mustre de Leon, S. I. Zabinsky, and R. C. Albers, "Theoretical X-ray Absorption Fine Structure Standards," *J. Am. Chem. Soc.*, **113,** 5135 (1991).

[15]D. K. Smith and H. W. Newkirk, "The Crystal Structure of Baddeleyite (Monoclinic ZrO_2) and Its Relation to the Polymorphism of ZrO_2," *Acta Crystallogr.*, **18,** 983–91 (1965).

[16]M. Faucher and J. Pannetier, "Reinforcement of the Y_2O_3 Structure at 77 K," *Acta Crystallogr.*, **B36,** 3209–11 (1980).

[17]S. Anderson, "The Crystal Structure of N-Nb_2O_5," *Inorg. Chem.*, **351,** 106–12 (1967).

[18]B. K. Teo, *EXAFS: Basic Principles and Data Analysis*. Springer-Verlag, New York, 1986.

[19]P. Li, I-W. Chen, and J. E. Penner-Hahn, "X-ray Absorption Studies of Zirconia Polymorphs. III. Static Distortion and Thermal Distortion," *Phys. Rev. B*, **48** [14] 10082–89 (1993).

[20]A. I. Komkov, "The Structure of Natural Fergusonite, and of a Polymorphic Modification," *Kristallografiya*, **4,** 836–41 (1959).

[21]I-W. Chen, Y. H. Chiao, and K. Tsuzaki, "Statistics of Martensitic Nucleation," *Acta Metall.*, **33,** 1827–45 (1985).

[22]J. C. J. Bart, "Near-Edge X-ray Absorption Spectroscopy in Catalysis," *Adv. Catal.*, **34,** 203–97 (1986).

[23]C. R. Natoli, "Distance Dependence of Continuum and Bound State of Excitonic Resonances in X-ray Absorption Near Edge Structure (XANES)"; pp. 442–44 in *EXAFS and Near Edge Structure III*. Edited by K. O. Hodgson, B. Hedman, and J. E. Penner-Hahn. Springer-Verlag, New York, 1984.

[24]P. Li, Y. Wang, and I-W. Chen, "Local Atomic Structures of $Pb(Zn_{1/3}Nb_{2/3})O_3$ and Related Perovskites. I. An XANES Study of Ionicity/Covalency," *Ferroelectricity*, in press.

[25]R. D. Shannon, "Revised Effective Ionic Radii and Systematic Studies of Interatomic Distances in Halides and Chalcogenides," *Acta Crystallogr.*, **A32,** 751–67 (1976).

[26]V. S. Stubican, "High-Temperature Transitions in Rare-Earth Niobates and Tantalates," *J. Am. Ceram. Soc.*, **47,** 55–58 (1964).

[27]H. P. Rouksby and E. A. D. White, "The Structures of 1:1 Compounds of Rare Earth Oxides with Niobia and Tantala," *Acta Crystallogr.*, **16,** 888 (1963).

[28]J. Lefevre, "Fluorite-Type Structural Phase Modifications in Systems Having a Zirconium or Hafnium Oxide Base," *Ann. Chim.*, **8,** 117–49 (1963).

[29]A. Ennaciri, D. Michel, M. Perez y Torba, and J. Pannetier, "Neutron Diffraction Determination of the Structure of an Ordered Scheelite-Type: Zr_5GeO_8," *Mater. Res. Bull.*, **19,** 793–99 (1984).

[30]M. Yoshimura, M. Yashima, T. Noma, and S. Somiya, "Formation of Diffusionlessly Transformed Tetragonal Phases by Rapid Quenching of Melts in ZrO_2-$RO_{1.5}$ Systems (R = Rare Earth)," *J. Mater. Sci.*, **25,** 2011–16 (1990). □